

Neural Networks and Friction: Slide, Hold, Learn

Joaquin Garcia-Suarez^{a)}

*Institute of Civil Engineering, École Polytechnique Fédérale de Lausanne (EPFL)
CH 1015 Lausanne, Switzerland*

(Dated: 26 February 2024)

In this study, it is demonstrated that Recurrent Neural Networks (RNNs), specifically those utilizing Gated Recurrent Unit (GRU) architecture, possess the capability to learn the complex dynamics of rate-and-state friction laws from synthetic data. The data employed for training the network is generated through the application of traditional rate-and-state friction equations coupled with the aging law for state evolution. A novel aspect of our approach is the formulation of a loss function that explicitly accounts for initial conditions, the direct effect, and the evolution of state variables during training. It is found that the RNN, with its GRU architecture, effectively learns to predict changes in the friction coefficient resulting from velocity jumps, thereby showcasing the potential of machine learning models in understanding and simulating the physics of frictional processes.

Keywords: friction, rate-and-state-dependent friction, neural networks, recurrent neural networks, GRU

I. INTRODUCTION

Understanding the dynamics of friction is paramount across several disciplines, including mechanical engineering, civil engineering, and geophysics^{1,2}. In mechanical and civil engineering, precise knowledge of frictional forces is crucial for the design and analysis of machines, structures, and materials under varying operational conditions^{3,4}. In geophysics, friction dynamics play a critical role in earthquake mechanics, influencing the initiation, propagation, and arrest of seismic slips along faults⁵.

Friction modeling^{6,7} aims to capture essential features observed in experimental settings⁸, notably the direct effect and healing². The direct effect refers to the immediate change in frictional resistance to a sudden change in sliding velocity. This phenomenon can be described by the empirical equation⁵:

$$\mu = \mu_0 + a \log \left(\frac{V}{V_{ref}} \right), \quad (1)$$

where μ is the friction coefficient, μ_0 is the friction coefficient at a reference velocity V_{ref} , V is the sliding velocity, and a is a positive constant representing the direct effect's sensitivity to velocity changes⁹.

Healing, also referred to as state evolution effect, illustrates the time-dependent increase in frictional resistance during stationary contact, attributed to the contact area's growth at asperity contacts or chemical bonding at the interface². This process is often modeled by the evolution of an internal variable θ (termed "state"), with the simplest form being:

$$\dot{\theta} = 1 - \frac{\theta V}{D_c}, \quad (2)$$

where D_c is a critical slip distance over which the state variable evolves significantly¹⁰. The state is interpreted as a measure of effective age of contacts between the asperities of the opposed surfaces^{9,11}, and it therefore has units of time. Equation (2) is termed "aging law".

Numerous models have been proposed to describe frictional behavior, from classical laws like Amontons-Coulomb friction², which simplifies friction as a constant proportion of the normal load, to more complex models incorporating velocity and time-dependent effects. However, these models often fall short in capturing the full range of observed behaviors^{5,12}.

Rate-and-state friction (RSF) laws stand out by explicitly addressing the direct effect and healing, thereby providing a more comprehensive framework for understanding the seismic cycle¹³. A customary expression of this law is⁵:

$$\mu = \mu_0 + a \ln \left(\frac{V}{V_{ref}} \right) + b \ln \left(\frac{V_{ref} \theta}{D_c} \right), \quad (3)$$

where b is a constant that, along with a , determines the frictional response to changes in sliding velocity and state evolution¹⁴. Despite their advantages, RSF laws are not without limitations. Identifying the parameters a , b , and D_c from experimental data poses significant challenges due to the complex interplay between different physical processes at the frictional interface⁵.

Criticism has been levied against the use of the "state" variable in RSF laws for its empirical nature and lack of a clear physical basis, leading to calls for models that include more explicit physical mechanisms^{15,16}. To begin, the parameters that appear in eq. (3) are assumed to be constants, and they may not¹⁷⁻²¹. Furthermore, the need to regularize these laws to address numerical instabilities and ensure the physical realism of simulations has



FIG. 1 Artistic representation of the magnified rough interface between two plates in sliding contact, where asperities grinding give rise to debris particle formation.

been highlighted^{22,23}. Recently, laboratory²⁴ and virtual experiments^{25,26} have shown the limitations of RSF laws even in highly controlled interface conditions.

Given these challenges and the limitations of existing models, there is a clear need to explore new methodologies for understanding friction dynamics. This necessity is particularly acute for modeling phenomena that span multiple scales of time and space²⁷. Herein lies the potential of leveraging advanced computational approaches, such as Recurrent Neural Networks (RNNs)²⁸, to offer new insights and overcome the limitations of traditional friction laws.

Neural networks have revolutionized the field of machine learning, offering powerful tools for modeling complex, non-linear relationships in data across a myriad of disciplines²⁹. At their core, neural networks are composed of layers of interconnected nodes or "neurons," each capable of performing simple computations. Through the process of training, these networks adjust their internal parameters to minimize the difference between their output and the desired outcome, effectively learning to map inputs to outputs³⁰.

Among the various architectures of neural networks, Recurrent Neural Networks (RNNs) stand out for their ability to process sequential data. Unlike feedforward neural networks, RNNs possess a form of memory that allows them to incorporate information from previous inputs into the current processing step³¹. This characteristic makes RNNs particularly suited for tasks involving time series data or any context where the sequence of data points is crucial.

Two notable advancements in RNN architecture are the Gated Recurrent Unit (GRU) and Long Short-Term Memory (LSTM) networks. Both GRU and LSTM address a fundamental limitation of basic RNNs known as the vanishing gradient problem, which makes it difficult for RNNs to learn dependencies between events that occur at long intervals in the input data³⁰. GRUs simplify the LSTM architecture while retaining its ability to capture long-term dependencies, making it both efficient and

powerful for a wide range of tasks³¹.

The application of RNNs, GRUs, and LSTMs has been widespread and transformative across many fields, including physics³². Particularly, their success in modeling path-dependent plasticity of materials highlights their potential³³⁻³⁷. Path-dependent plasticity is a critical aspect in the study of materials science, where the history of material deformation affects its current and future state. RNNs have been shown to effectively model these complex relationships, capturing the history-dependent nature of material behavior^{38,39}.

This success in modeling path-dependent phenomena in materials science provides a strong foundation for the belief that similar methodologies can be applied with success to the study of friction. Friction, much like material plasticity, is inherently dependent on history, in its case of contact and slip between surfaces. The capability of RNNs to capture and learn from sequential, history-dependent data makes them promising candidates for advancing our understanding and modeling of friction dynamics.

The goal of this short communication is to show that RNNs, based on GRUs, can perform at least *as well as* RSF laws, the aging law in particular, eq. (2). This approach is essentially different from the one used recently by Ishiyama and collaborators⁴⁰, who used machine learning (random forest⁴¹) to improve the estimation of RSF parameters eq. (3): machine learning is not deployed to improve an empirical approximate law, but to replace it altogether, down the road, in larger-scale simulations^{16,42,43}. It also differs from the use made by Rouet-Leduc *et al*⁴⁴ and Hulbert *et al*⁴⁵, among others^{46,47}, who used machine learning techniques to devise impending rupture predictions based on acoustic emissions recorded in lab settings. Herein, we assume a virtual interface that is perfectly modeled by a traditional slip-law eqs. (2) and (3), for which data for training and verification can be generated easily. We use those data to train a custom GRU network that learns the dynamics without internal variables, since the state is not a physical quantity that can be measured experimentally (assuming it even exists as such). In reality, the complexities of interface physics⁴⁸ are such that probably no simplified internal variable can be defined as long as one aims at capturing any modestly ambitious degree of complexity. We presume implicitly that sliding amount and sliding rate are the sole driving forces of the phenomenon, and whatever internal variables there may be can be internally codified in the parameters of the net. The figure of merit will not be the dynamic friction coefficient itself, but *variations in the friction coefficient* due to sliding. This decision is motivated by the practical inability to surmise the time evolution of the friction coefficient except if proper initial conditions are supplied.

The structure of the paper is as follows: the methods section (1) introduces the GRU architecture, (2) describes the generation of synthetic data for training and verification, and (3) explains the choice of training hyper-

parameters, including the physics-informed loss function. The next section describes the outcome of the training process, which details performance evaluation, and then assesses the model’s predictive accuracy on independent datasets. The discussion section analyzes the findings and their implications. The final remarks section summarizes the study’s contributions and suggests future research directions.

II. METHODS

II.A. Neural networks for sequences: gated recurrent units

RNNs are engineered to handle sequential data thanks to their ability to maintain a memory of previous inputs by feeding the output of a neuron back onto itself²⁸. This recursive nature allows making predictions based on the information accumulated from prior inputs. However, standard RNNs often struggle with long-term dependencies due to the vanishing gradient problem³⁰, where gradients become too small or too large for the network to learn effectively over many time steps.

Gated Recurrent Units (GRUs) are an evolution of the traditional RNN architecture, designed to mitigate the vanishing gradient problem and improve the network’s ability to learn from long sequences. GRUs introduce gating units that control the flow of information. These gates “decide” which information is relevant to keep or discard as the sequence progresses, enabling the network to maintain a longer memory.

The GRU mechanism is articulated mathematically through³¹:

- Update gates:

$$z_t = \sigma(W_z x_t + U_z h_{t-1} + \xi_z). \quad (4)$$

- Reset gates:

$$r_t = \sigma(W_r x_t + U_r h_{t-1} + \xi_r). \quad (5)$$

- Candidate states:

$$\tilde{h}_t = \tanh(W x_t + U(r_t \odot h_{t-1} + \xi)). \quad (6)$$

- Final state updates:

$$h_t = (1 - z_t) \odot h_{t-1} + z_t \odot \tilde{h}_t. \quad (7)$$

In these equations, x_t represents the input at time step t ; h_t is the hidden state at time t ; σ denotes the sigmoid activation function (to ensure the gate activations are constrained between 0 and 1); \tanh is the hyperbolic tangent function (introducing non-linearity); W , U , and ξ are the weights and biases associated with the input and hidden states, respectively; and \odot signifies element-wise multiplication.

By merging the forget and input gates into a single update gate, GRUs simplify the LSTM architecture, reducing the model’s complexity and computational demands while maintaining robust performance.

II.B. Synthetic data generation

As mentioned earlier, it is assumed that the state θ will not be needed by the neural network that is to replace the traditional RSF law. This means that there will not be vectors of values of θ being used during training and that the network will not , but it does not imply that eq. (2) is not being used during the datasets’ generation. Let us reiterate that we assume a hypothetical interface that is perfectly described by eq. (3) in tandem with eq. (7), but this fact would be hidden to us if we were to analyze experimental data coming out of that interface.

So, to generate the dataset for training and verifying our model, we start by defining a traditional RSF model with specific parameter values, grounded in the fundamental equations presented earlier (eq. (3)), with parameter values set as follows:

- Friction coefficient, $\mu_0 = 0.5$ (unitless)
- Rate-state parameter, $b = 0.015$ (unitless)
- Direct effect parameter, $a = 0.005$ (unitless)
- Reference velocity, $V_{\text{ref}} = 1.0 \cdot 10^{-4}$ m/s
- Characteristic slip distance, $D_c = 2.0 \cdot 10^{-4}$ m

Using these values, we simulate 15000 random sequences to reflect diverse frictional sliding scenarios. Each sequence is designed to simulate a total sliding distance of $30D_c$ and is completed within 0.013 seconds. The number of velocity jumps within each sequence is randomly determined, drawing from a uniform distribution with values 2, 3, 4, 5. It is assumed that each sequence initiates from a non-zero velocity, with the initial state of the interface corresponding to the steady state for that velocity, as defined by the RSF laws: $\theta_{ss} = D_c/V(t=0)$.

Velocity jumps within these sequences occur at random intervals, determined by sampling times from a uniform distribution across the interval 0, 1, with 0 marking the start and 1 the end of the sliding protocol. Each sequence incorporates a hold period where the velocity drops to zero, simulating intervals where sliding stops until the subsequent jump. To avoid errors associated to dividing by zero or trying to compute the logarithm of zero, a tiny yet finite velocity is assigned to the hold for computations ($2 \cdot 10^{-9}$ m/s).

To compute the velocities between jumps, we divide the total sliding distance by the time spans between these jumps, ensuring that the velocities remain constant in these intervals. Thus, we define the “velocity protocol” for each sequence / virtual experiment.

Having the velocity protocol, we proceed to calculate the evolution of the state variable θ using eq. (2) and initial conditions $V(t=0) = V_0$ and $\theta(t=0) = \theta_{ss}$. With the velocity protocol and the evolving state variable at hand, we can then compute the friction coefficient’s evolution over time, as described by the RSF model (eq. (3)).

The dataset comprises pairs of “features” and “targets”. Features represent the velocity protocol sampled

at 100 equally-spaced instants during the duration of each virtual experiment, while targets correspond to *variations* of the friction coefficient sequence at these same instants. What is the reason for working with variations and not with the actual values of friction coefficient? There is no way to predict the initial values of friction based on these datasets, they have to be provided as initial conditions over which the variations are later superimposed.

For training, we normalize using the following characteristic values: $\delta\mu_{ch} = 0.01$ for the friction coefficient change and $V_{ch} = 0.3$ m/s for the velocities. 20% of the sequences are put aside to test the network once it is trained.

II.C. Network details

Mathematica's⁴⁹ neural networks package has been used.

II.C.1. Architecture

The main net, which is aimed at replacing eq. (3) and whose parameters must be learned via training, is made up by a `GatedRecurrentLayer`, followed by a folded `LinearLayer` to transform the output of the GRU through a linear transformation.

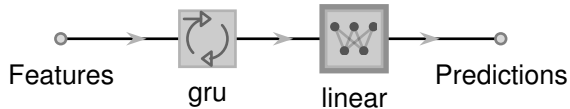


FIG. 2 Scheme of main part of the network

II.C.2. Training parameters

We employ the ADAM optimization method⁵⁰ due to its adaptive learning rate capabilities, which helps in converging to the optimal solution more quickly and efficiently than conventional gradient descent methods. A learning rate of 0.001 is chosen as a starting point because it strikes a balance between fast convergence and the risk of overshooting the minimum of the loss function. This value is generally considered a good default and has been proven effective across a wide range of tasks. In order to ensure that each training batch has enough data to represent the dataset's diversity while keeping the computational demand manageable, we choose to use a batch size of 32. Finally, we use 50 epochs to allow the model opportunity to learn from the data without excessive training time.

II.C.3. Loss function

Inspired by physics-informed neural networks (PINNs)³², we devise a loss function that reflects physical principles to guide the optimization of the

parameters of the network. The conditions that observations impose over the friction coefficient are the direct effect, i.e., logarithmic dependence of velocity magnitude, and healing, i.e., logarithmic increase of the static friction coefficient with time (during holds)

$$\frac{\partial\mu}{\partial\log V} = c_1, \quad \frac{\partial\mu}{\partial\log t} = c_2, \quad (8)$$

where μ_s is the static friction coefficient, c_1 and c_2 are interface-dependent constants. The latter correspond to a and $(a - b)$ (eq. (3)), but we are assuming we do not know that the interface is modeled by these parameters, so shall impose that the change of these relative variations is constant, not that the variations themselves are of a given magnitude. There seems to be a real possibility²⁰ that these constants may change over time, so, to adapt the framework to this fact, we chose not to enforce the same constants over all the protocols but individually for each sequence, by not mixing information from other different series.

Apart from these two conditions, we must impose that there are no variations until the first jump (as we took for granted that each experiment starts from steady-state conditions) and that the average error is small, in order for the prediction to follow also the general trend in the target data.

Let $\delta\boldsymbol{\mu}$ and $\delta\hat{\boldsymbol{\mu}}$ represent the vector of normalized predictions and targets (respectively) for a given vector of features (velocity protocol) \mathbf{V} , i.e., $\delta\boldsymbol{\mu} = \text{NN}(\mathbf{V}/V_{ch})$. See that $\delta\boldsymbol{\mu}, \delta\hat{\boldsymbol{\mu}}, \mathbf{V} \in \mathbb{R}^N$ (and $N = 100$ in this case). The first part of the loss is the mean-squared error:

$$\text{loss}_1 = \frac{\|\delta\boldsymbol{\mu} - \delta\hat{\boldsymbol{\mu}}\|_2^2}{N}, \quad (9)$$

where $\|\cdot\|$ represents the L_2 norm of the vector. In overall graph for training, fig. 6, this operation is implemented by the neuron labeled MS.

The second part of the loss represents the difference between the initial values of predictions and targets,

$$\text{loss}_2 = (\delta\mu_1 - \delta\hat{\mu}_1)^2, \quad (10)$$

where the sub-index 1 refers to the first element of every sequence. The implementation of this operation is depicted in fig. 3: it takes the first sequence value of both targets (`Targets`) and predictions (`Predictions`), subtracts each other and squares the difference. Thus, the output of the net is eq. (10).

The third term of the loss is meant to enforce the direct effect: a sudden peak in friction induced by a jump in leading velocity (which, moreover, is known to be proportional to the logarithm of the ratio of velocities before and after the jump, see section I and appendix A). Assume that there are N_J jumps in a given protocol, the term that measures the error between the one predicted by the network and the real one is

$$\text{loss}_3 = \sum_{i=1}^{N_J} \{\Delta(\delta\mu)_{J_i} - \Delta(\delta\hat{\mu})_{J_i}\}^2, \quad (11)$$

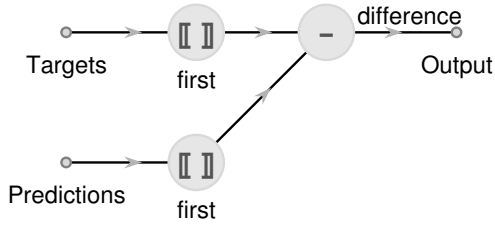


FIG. 3 Scheme of sub-net that implements comparison of initial condition.

the symbol i indexes each jump, while J_i refers to the entry of the vector where the jump begins, hence the meaning of the notation $\Delta(\delta\mu)_{J_i} = \delta\mu_{J_i+1} - \delta\mu_{J_i}$. The network depicted in fig. 4 implements this procedure: the inputs are the predictions generated by the GRU net (fig. 2) **Predictions**, the indices of the entries where velocity jumps begin **PosBeforeJ** and after **PosAfterJ**, and the real magnitude of the friction jump ΔF_{data} , the output is the evaluation of eq. (11).

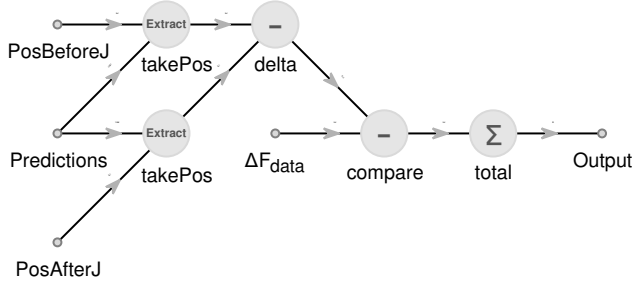


FIG. 4 Sub-net that implements direct effect.

Finally, interface strengthening during hold periods (a.k.a. healing) is recognized to happen logarithmically with respect to hold time, i.e., counting from the moment that the interface ceases to move. Consider that, given a sequence, the hold period starts at the j -th entry, and it lasts until $(j + N_h)$ -th entry. We can gather these terms in a separate vector $\delta\mu_h = \{\delta\mu_i\}_{i=k}^{i=k+N_h} = \{\delta\mu_n\}_{n=1}^{n=N_h}$, where the sub-index n has been introduced to index the values during hold straightforwardly. So the healing condition can be expressed as:

$$\frac{\delta\mu_n - \delta\mu_{N_h}}{\log\left(\frac{n}{N_h}\right)} = \text{constant} \quad \forall n = 1, \dots, N_h - 1. \quad (12)$$

Thus, the loss term is:

$$\text{loss}_4 = \sum_{n=1}^{N_h-2} \left\{ \frac{\delta\mu_{n+1} - \delta\mu_{N_h}}{\log\left(\frac{n+1}{N_h}\right)} - \frac{\delta\mu_n - \delta\mu_{N_h}}{\log\left(\frac{n}{N_h}\right)} \right\}^2. \quad (13)$$

This loss term is realized schematically as in fig. 5. The first input is again **Predictions**, coming from the main network fig. 2, the second one is N_h , which is the position of the entry where the hold ends, it is necessary

to extract the predicted value $\delta\mu_{N_h}$. The latter is then replicated to form a vector that is subtracted to all predictions. The final input **LogTerms** weights the healing values as per eq. (12) and “masks” the not-healing ones since it contains zeros that multiply those entries. Once the vector has been weighted, two copies of it are made, shifted to compare successive entries and then summed and squared, yielding as output eq. (13).

The overall loss term that guides the optimization of weights and biases during the training process is:

$$\text{loss} = \text{loss}_1 + \alpha\text{loss}_2 + \beta\text{loss}_3 + \gamma\text{loss}_4, \quad (14)$$

$\alpha, \beta, \gamma \in \mathbb{R}$. It has been found that $\alpha = 1$, $\beta = 0.1$ and $\gamma = 5 \cdot 10^{-3}$ yields satisfactory results, yet probably not optimal (see discussion section).

III. TRAINING RESULTS

The training was performed in Mathematica⁴⁹, using the architecture and hyperparameters discussed in section II and 12000 random sequences corresponding to virtual protocols.

The overall training procedure is depicted in fig. 7 and the final losses are consigned in table I. The complex loss function eq. (13) was not used at once, but an incremental approach was explored: first, the simplest loss (mean squared error, ME) was used to initialize weights and biases. Second, the network was retrained adding the initial-condition term (ME + ics), which further reduced the loss by 50%. This main part was again extracted and used into a larger scheme that included the direct effect loss term (ME + ics + de). The overall precision suffered, but, as it will be shown, this deterioration of the objective function minimization does not translate into a substantial deterioration of the overall approximation; rather, it seems that this larger value reflects the struggle to capture the jumps’ magnitude. We tried re-training the network from ME + ics for both direct effect and healing simultaneously (ME + ics + de + heal), to no avail. Apparently, the addition of the healing phenomenology to the loss further deflects from the optimum, but it is believed that this is really a drawback of the RSF model used to generate the synthetic data.

TABLE I Final loss value for different loss functions: ME refers to mean squared error between predictions and targets, ICs refers to enforcing the first value of predictions to be equal to targets’, DE does to enforcing friction jumps in target data and predictions to be of the same magnitude, H refers to enforcing logarithmic healing.

ME	ME+ICs	ME+ICs+DE ⁵¹	ME+ICs+DE+H ⁵²
0.064	0.033	0.255	0.271

IV. TEST

Once the training is complete, we take out the main net, which is our ready-to-use NN function that is to model the interface evolution. We test it using the 3000

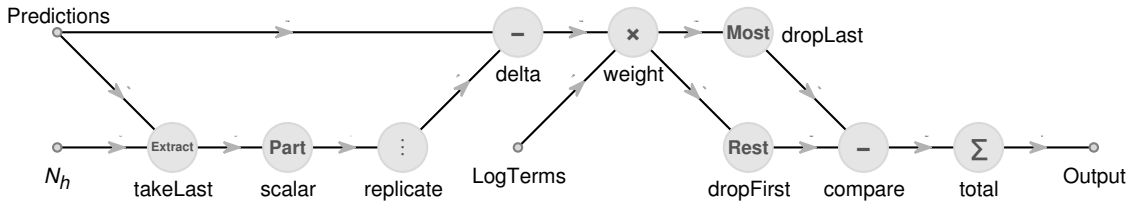


FIG. 5 Sub-net that implements logarithmic healing during holds.

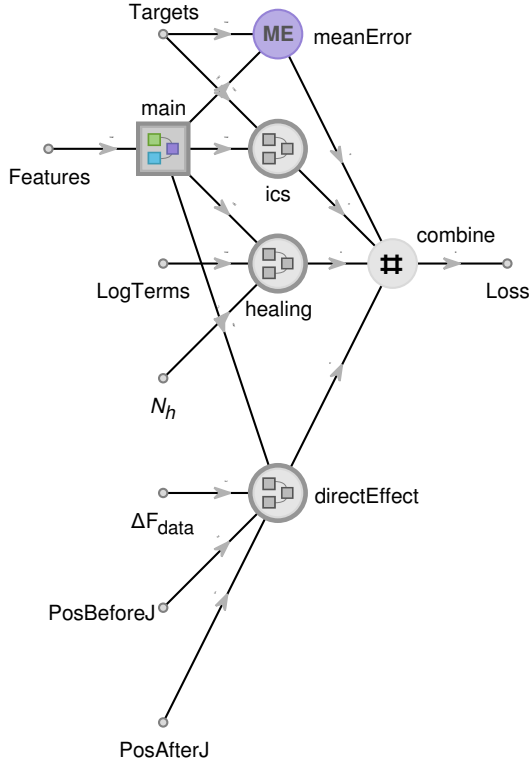


FIG. 6 Scheme of the global training network

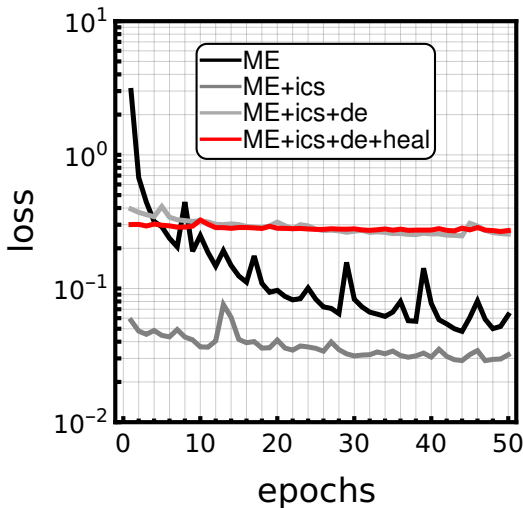


FIG. 7 Mean training loss: ME is trained without initialization, ME + ics is trained with parameters from ME, ME + ics + de and ME + ics + de + heal are trained with parameters from ME + ics.

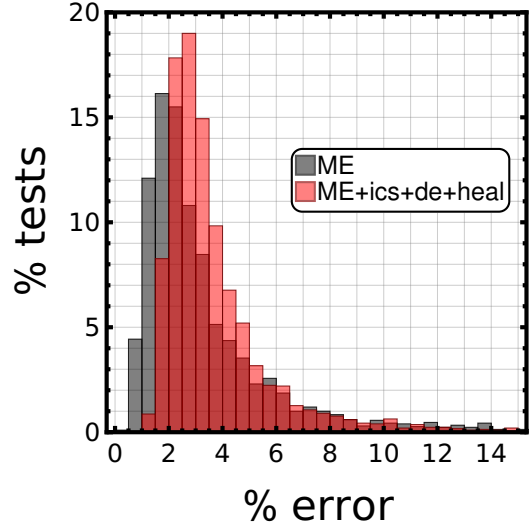


FIG. 8 Verification error breakdown: percentage of test cases that yield a certain percent error.

sequences that the net did not see during training. For each sequence, the percent error is computed as

$$\text{error}(\%) = 100 \frac{\|\text{NN}(\mathbf{V}/V_{ch}) - \delta \hat{\boldsymbol{\mu}} / \delta \mu_{ch}\|_2}{\|\delta \hat{\boldsymbol{\mu}} / \delta \mu_{ch}\|_2}. \quad (15)$$

The mean test error (averaged over the 3000 sequences) is consigned in table II for the four different architectures discussed above. It remains fairly constant, always below 5%, the minimum being attained for the loss combining the averaged square error for the whole vector with the direct enforcement of zero change at $t = 0$. Their accuracy can be directly grasped in figs. 9 and 10, which will be commented in the next section.

Finally, fig. 8 compares the error distribution across sequences for both the simplest network and the most complex one. In the latter case, the most current error is $\sim 3\%$ (19% of tests), while $\sim 2\%$ (16% of tests) in the former.

TABLE II Mean test error (%) for different loss functions (see table I for labels' explanation).

ME	ME+ICs	ME+ICs+DE	ME+ICs+DE+H
4.2	3.4	3.655	4.1

V. DISCUSSION

As hinted by the test results presented in table II, figs. 9 and 10 clearly showcase that the GRU-based network NN is able of closely reproducing the friction dynamics encapsulated in the datasets generated with a customary rate-and-state phenomenological law.

Nevertheless, there are obvious limitations. First, the inset in fig. 9 reveals that the enforcement of the initial condition prevents an initial substantial error, but it does not prevent oscillations even though the velocity remains constant. This issue is deemed of minor importance, since real interface data will certainly come with small levels of noise that the network must filter through. By the way, at this point we will have to consider also the use of regularization to prevent overfitting, a feature that was not necessary as the datasets were noiseless.

The fact that the target (friction coefficient) changes during the steady state when there is no change in the features (loading velocities) is a clear drawback, no matter how slightly the change may be.

Moreover, the absence of the state variable in the dataset brings about inaccuracies in reproducing behavior during holds, despite (or rather, because of) explicitly implementing logarithmic healing in the objective function. Logarithmic healing, eq. (8), entails that the increment of static friction coefficient $\Delta\mu_s$ over a timespan Δt abides by

$$\Delta\mu_s \propto \frac{\Delta t}{t}, \quad (16)$$

where t is the total time elapsed from the arrest. Conversely, if we integrate eq. (2) and then plug it back into eq. (3), a term depending on the initial value of the state variable appears:

$$\Delta\mu_s \propto \frac{\Delta t}{\theta(t=0) + t}, \quad (17)$$

which can interfere with the scaling, unless $\theta(t=0) \ll t$. The latter condition may be met in real experiments, in which the holds tend to last for much longer than the characteristic age of the interface, but it is certainly not the case here as the holds are always “short”, i.e., of duration similar to the magnitude of the state variable. This seems to be the most obvious drawback of not considering explicitly the interface state in the data-driven framework. In any case, it does not appear as insurmountable, since (as justified above) in real data the behavior during periods of rest would adjust better to the logarithmic scaling.

Yet another aspect to acknowledge is that the magnitude of direct effect peaks seems to be affected by the holds. See for instance that in fig. 9 there is a relatively short hold period preceded and ended by jumps which are well captured by the nets; conversely, the jumps’ magnitude are significantly underpredicted in fig. 10, which features a longer hold, particularly by the net tuned explicitly for healing.

Some of these issues could be remedied drawing inspiration from PINNs³² again, by taking advantage of

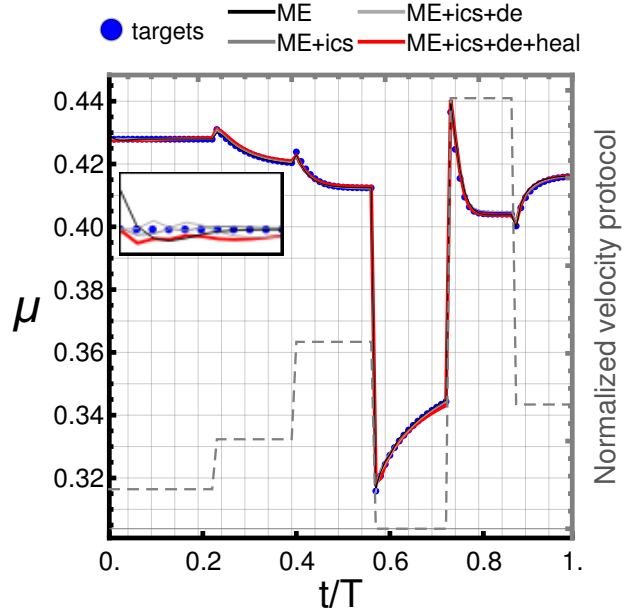


FIG. 9 Test example #1: light left axis for loading velocity, dark right axis for friction coefficient evolution. Emphasis on initial conditions. The dashed background line represents the velocity protocol. Protocol with hold playing a secondary role.

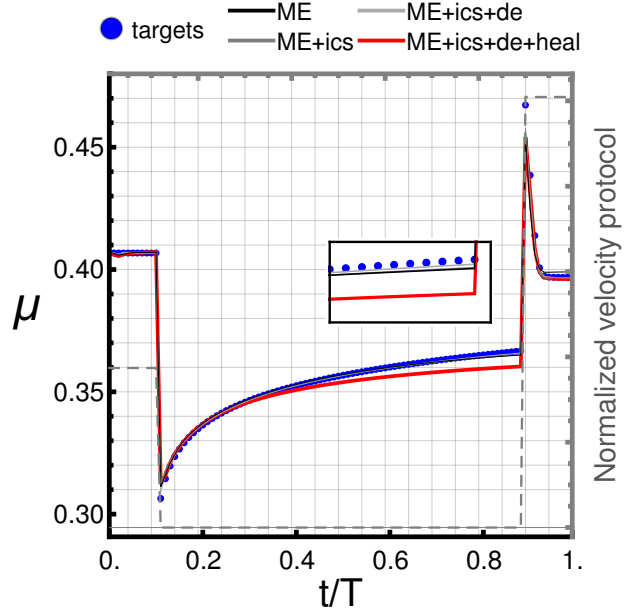


FIG. 10 Test example #2: light left axis for loading velocity, dark right axis for friction coefficient evolution. Emphasis on shortcomings in healing and direct effect. The dashed background line represents the velocity protocol. Protocol with relevant hold.

the automatic differentiation⁵³ to automatically compute gradients of the friction coefficient (output) as a function of the velocities (input) so that they can be directly monitored during training. Not only that, it is logical to expect that automatic differentiation can also enable more elegant approaches to implementing both direct effect and healing in the loss function.

VI. FINAL REMARKS

This study has demonstrated that recurrent neural networks based on Gated Recurrent Units (GRUs) possess the capability to accurately model slide-hold protocols in the context of rate-and-state friction laws, provided that the networks are supplied with adequate data and the loss function is tuned accordingly. Our findings affirm the potential of recurrent neural networks as a powerful tool for understanding complex frictional behavior, showcasing their ability to learn from and predict the dynamics of friction with high fidelity. This success highlights the ability of deep learning approaches to replace customary phenomenological laws for dynamic friction, additionally avoiding the need to define internal variables.

However, our investigation also identified limitations, particularly concerning the handling of logarithmic healing during hold periods. Additionally, we observed a potential conflict between optimizing for healing and for the direct effect within the training process, indicating an area for further refinement in how these fundamental aspects of frictional behavior are integrated into the learning scheme. And let alone that no noise has been included in the training datasets yet, and only protocols made of sudden velocity jumps changes were considered.

This document contains but an exploratory approach to modeling frictional interface via deep learning. Looking forward, there are several promising avenues for enhancing the predictive power and generalizability of recurrent neural networks for dynamic friction. Improvement could be sought through the exploration of alternative RNN architectures and more nuanced physics-informed loss functions (for instance, to account for friction manifesting indirectly in the dynamics of spring-block systems²). Further parametric studies in terms of network hyperparameters are also warranted, in particular in terms of volumes of available data: unlike cheap synthetic data, experimental data remains relatively scarce; hence it is worth exploring how new techniques^{54,55}, aimed at improving data economy in the context of constitutive modeling with neural networks, can help in this case.

As mentioned above, incorporating spring-block dynamics into the model could pave the way for learning from real experimental data, thus circumventing the gap between theoretical models and practical observations. Combined with the use of automatic differentiation⁵³ (not explored at this point), it could offer a completely new pathway to take advantage of laboratory results to understand friction, replacing the use of experiments to simply fit parameters by producing training data that is the infused in a network that can be used later for predictions.

Moreover, the exploration of advanced machine learning features such as transformers⁵⁶ and Long Short-Term Memory (LSTM) networks⁵⁷ could offer additional improvements. These technologies, known for their ability to capture long-distance dependencies within data, might

provide the key to overcoming some of the current limitations. The promise of deep learning does not stop there: one can foresee that an approach based on neural *operators*⁵⁸ may help also with the problem of generalizing friction from lab conditions to crustal ones.

The end goal is to evolve from traditional phenomenological friction models towards more accurate representations that are likewise derived from the data already used for parameter fitting. This evolution does not entail giving up on a deeper understanding of friction dynamics. Rather, it calls for a complementary integration of solid physical principles with the deep learning paradigm. The rationale for adopting these deep-learning models shall be their demonstrable ability to accurately capture complex interface physics, which, in turn, would justify their use in larger-scale numerical simulations involving those phenomena.

ACKNOWLEDGEMENTS

The author acknowledges financial support from the Swiss National Science Foundation, via Ambizione Grant PZ00P2.216341 “Data-Driven Computational Friction”. Useful conversations (regarding text improvements, rate-and-state friction and/or laboratory experiments) with Dr. Gabriel Meyer, Dr. Simon Guérin-Marthe and Ms. Roxane Ferry are gratefully acknowledged. An EPFL bachelor project conducted by Mr. Antoine Binggeli provided Tensorflow code that inspired the use of GRUs to this particular problem.

Finally, this paper not only verses on but also benefited from artificial intelligence: the artwork in the introduction (fig. 1) was generated using DALL-E and GPT-4 has provided both help with and input to the text.

DATA AVAILABILITY

The notebooks used to generate both data and results in this paper are available via correspondence with the author (joaquin.garciasuarez@epfl.ch).

REFERENCES

- a) Electronic mail: joaquin.garciasuarez@epfl.ch
- ¹E. Rabinowicz, “The Nature of the Static and Kinetic Coefficients of Friction,” *Journal of Applied Physics* **22**, 1373–1379 (1951).
- ²C. H. Scholz, *The mechanics of earthquakes and faulting* (Cambridge university press, 2019).
- ³Z. Bažant and B. Oh, “Crack band theory for fracture of concrete,” *Materials and Structures* **16**, 155–177 (1983).
- ⁴P. K. Mehta and P. J. Monteiro, *Concrete: Microstructure, Properties, and Materials*, 4th ed. (McGraw-Hill Education, New York, NY, 2014).
- ⁵C. Marone, “Laboratory-derived friction laws and their application to seismic faulting,” *Annual Review of Earth and Planetary Sciences* **26**, 643–696 (1998).
- ⁶K. L. Johnson, *Contact Mechanics* (Cambridge University Press, Cambridge, UK, 1985).
- ⁷A. Bizzarri, “On the deterministic description of earthquakes,” *Reviews of Geophysics* **48** (2010).

- ⁸N. M. Beeler, T. E. Tullis, M. L. Blanpied, and J. D. Weeks, “Frictional behavior of large displacement experimental faults,” *Journal of Geophysical Research: Solid Earth* **101**, 8697–8715 (1996), <https://agupubs.onlinelibrary.wiley.com/doi/pdf/10.1029/96JB004113>
- ⁹J. Dieterich, “Modeling of rock friction: 1. experimental results and constitutive equations,” *Journal of Geophysical Research* **84**, 2161–2168 (1979).
- ¹⁰C. Marone and B. Kilgore, “Scaling of the critical slip distance for seismic faulting with shear strain in fault zones,” *Nature* **362**, 618–621 (1993).
- ¹¹J. H. Dieterich and B. D. Kilgore, “Direct observation of frictional contacts: New insights for state-dependent properties,” *Pure and applied geophysics* **143**, 283–302 (1994).
- ¹²J. Woodhouse, T. Putelat, and A. McKay, “Are there reliable constitutive laws for dynamic friction?” *Philosophical Transactions of the Royal Society A: Mathematical, Physical and Engineering Sciences* **373**, 20140401 (2015).
- ¹³J. Rice and Y. Ben-Zion, “Slip complexity in earthquake fault models,” *Proceedings of the National Academy of Sciences* **93**, 3811–3818 (1996).
- ¹⁴A. Ruina, “Slip instability and state variable friction laws,” *Journal of Geophysical Research: Solid Earth* **88**, 10359–10370 (1983).
- ¹⁵J. R. Rice and A. L. Ruina, “Constitutive relations for fault slip and earthquake instabilities,” *Pure and Applied Geophysics PA-GEOPH* **121**, 443–475 (1983).
- ¹⁶N. Lapusta, J. R. Rice, Y. Ben-Zion, and G. Zheng, “Elastodynamic analysis for slow tectonic loading with spontaneous rupture episodes on faults with rate- and state-dependent friction,” *Journal of Geophysical Research: Solid Earth* **105**, 23765–23789 (2000).
- ¹⁷H. Noda and N. Lapusta, “Stable creeping fault segments can become destructive as a result of dynamic weakening,” *Nature* **493**, 518–521 (2013).
- ¹⁸D. M. Veeu and S. Barbot, “The parkfield tremors reveal slow and fast ruptures on the same asperity,” *Nature* **532**, 361–365 (2016).
- ¹⁹S. Xu, E. Fukuyama, F. Yamashita, K. Mizoguchi, S. Takizawa, and H. Kawakata, “Strain rate effect on fault slip and rupture evolution: Insight from meter-scale rock friction experiments,” *Tectonophysics* **733**, 209–231 (2018), physics of Earthquake Rupture Propagation.
- ²⁰Y. Urata, F. Yamashita, E. Fukuyama, H. Noda, and K. Mizoguchi, “Apparent dependence of rate- and state-dependent friction parameters on loading velocity and cumulative displacement inferred from large-scale biaxial friction experiments,” *Earthquakes and Multi-hazards Around the Pacific Rim, Vol. I*, 23–43 (2018).
- ²¹K. Im, D. Saffer, C. Marone, and J.-P. Avouac, “Slip-rate-dependent friction as a universal mechanism for slow slip events,” *Nature Geoscience* **13**, 705–710 (2020).
- ²²A. M. Rubin and J.-P. Ampuero, “Earthquake nucleation on (aging) rate and state faults,” *Journal of Geophysical Research: Solid Earth* **110** (2005).
- ²³Y. Bar-Sinai, E. A. Brener, and E. Bouchbinder, “Stable sliding and velocity-strengthening friction: Nucleation theory versus experiments,” *Geophysical Research Letters* **39** (2012).
- ²⁴A. Bizzarri, A. Petri, and A. Baldassarri, “Earthquake dynamics constrained from laboratory experiments: new insights from granular materials,” *arXiv preprint arXiv:2401.10595* (2024).
- ²⁵B. Ferdowsi and A. M. Rubin, “A granular physics-based view of fault friction experiments,” *Journal of Geophysical Research: Solid Earth* **125**, e2019JB019016 (2020), e2019JB019016 10.1029/2019JB019016.
- ²⁶B. Ferdowsi and A. M. Rubin, “Slide-hold-slide protocols and frictional healing in discrete element method (dem) simulations of granular fault gouge,” *Journal of Geophysical Research: Solid Earth* **126**, e2021JB022125 (2021), e2021JB022125 2021JB022125.
- ²⁷Y. Ben-Zion, “Dynamic ruptures in recent models of earthquake faults,” *Journal of the Mechanics and Physics of Solids* **49**, 2209–2244 (2001).
- ²⁸I. Goodfellow, Y. Bengio, and A. Courville, *Deep Learning* (MIT Press, 2016).
- ²⁹Y. LeCun, Y. Bengio, and G. Hinton, “Deep learning,” *Nature* **521**, 436–444 (2015).
- ³⁰S. Hochreiter and J. Schmidhuber, “Long short-term memory,” *Neural Computation* **9**, 1735–1780 (1997).
- ³¹K. Cho *et al.*, “Learning phrase representations using rnn encoder-decoder for statistical machine translation,” in *Proceedings of the 2014 Conference on Empirical Methods in Natural Language Processing (EMNLP)* (2014).
- ³²M. Raissi, P. Perdikaris, and G. Karniadakis, “Physics-informed neural networks: A deep learning framework for solving forward and inverse problems involving nonlinear partial differential equations,” *Journal of Computational Physics* **378**, 686–707 (2019).
- ³³M. Mozaffar, R. Bostanabad, W. Chen, K. Ehmann, J. Cao, and M. A. Bessa, “Deep learning predicts path-dependent plasticity,” *Proceedings of the National Academy of Sciences* **116**, 26414–26420 (2019).
- ³⁴Y. Heider, K. Wang, and W. Sun, “So(3)-invariance of informed-graph-based deep neural network for anisotropic elastoplastic materials,” *Computer Methods in Applied Mechanics and Engineering* **363**, 112875 (2020).
- ³⁵M. B. Gorji, M. Mozaffar, J. N. Heidenreich, J. Cao, and D. Mohr, “On the potential of recurrent neural networks for modeling path dependent plasticity,” *Journal of the Mechanics and Physics of Solids* **143**, 103972 (2020).
- ³⁶F. Masi, I. Stefanou, P. Vannucci, and V. Maffi-Berthier, “Thermodynamics-based artificial neural networks for constitutive modeling,” *Journal of the Mechanics and Physics of Solids* **147**, 104277 (2021).
- ³⁷H. J. Logarzo, G. Capuano, and J. J. Rimoli, “Smart constitutive laws: Inelastic homogenization through machine learning,” *Computer Methods in Applied Mechanics and Engineering* **373**, 113482 (2021).
- ³⁸C. Bonatti and D. Mohr, “One for all: Universal material model based on minimal state-space neural networks,” *Science Advances* **7**, eabf3658 (2021).
- ³⁹J. Dornheim, L. Morand, H. J. Nallani, and D. Helm, “Neural networks for constitutive modeling: From universal function approximators to advanced models and the integration of physics,” *Archives of Computational Methods in Engineering* (2023).
- ⁴⁰R. Ishiyama, E. Fukuyama, and B. Enescu, “Estimation of time-variable friction parameters using machine learning,” *Geophysical Journal International* **236**, 395–412 (2023).
- ⁴¹L. Breiman, “Random forests,” *Machine learning* **45**, 5–32 (2001).
- ⁴²N. Lapusta and J. R. Rice, “Nucleation and early seismic propagation of small and large events in a crustal earthquake model,” *Journal of Geophysical Research: Solid Earth* **108** (2003).
- ⁴³C. Cattania, S. Hainzl, F. Roth, and L. Wang, “The relationship between afterslip and aftershocks: A study based on coulomb-rate-and-state models,” *Journal Geophys. Res.* **16**, 5118 (2014).
- ⁴⁴B. Rouet-Leduc, C. Hulbert, D. C. Bolton, C. X. Ren, J. Riviere, C. Marone, R. A. Guyer, and P. A. Johnson, “Estimating fault friction from seismic signals in the laboratory,” *Geophysical Research Letters* **45**, 1321–1329 (2018).
- ⁴⁵C. Hulbert, B. Rouet-Leduc, P. A. Johnson, C. X. Ren, J. Riviere, D. C. Bolton, and C. Marone, “Similarity of fast and slow earthquakes illuminated by machine learning,” *Nature Geoscience* **12**, 69–74 (2019).
- ⁴⁶K. Wang, C. W. Johnson, K. C. Bennett, and P. A. Johnson, “Predicting future laboratory fault friction through deep learning transformer models,” *Geophysical Research Letters* **49**, e2022GL098233 (2022).
- ⁴⁷S. Karimpouli, D. Caus, H. Grover, P. Martínez-Garzón, M. Bohnhoff, G. C. Beroza, G. Dresen, T. Goebel, T. Weigel, and G. Kwiatek, “Explainable machine learning for labquake prediction using catalog-driven features,” *Earth and Planetary Science Letters* **622**, 118383 (2023).
- ⁴⁸A. Vakis, V. Yastrebov, J. Scheibert, L. Nicola, D. Dini, C. Minfray, A. Almqvist, M. Paggi, S. Lee, G. Limbert, J. Molinari, G. Ancaix, R. Aghababaei, S. Echeverri Restrepo, A. Papanagelo, A. Cammarata, P. Nicolini, C. Putignano, G. Carbone,

- S. Stupkiewicz, J. Lengiewicz, G. Costagliola, F. Bosia, R. Guarino, N. Pugno, M. Müser, and M. Ciavarella, “Modeling and simulation in tribology across scales: An overview,” *Tribology International* **125**, 169–199 (2018).
- ⁴⁹S. Wolfram, *The mathematical book*, Vol. 4 (Cambridge University Press Cambridge, 2000).
- ⁵⁰D. P. Kingma and J. Ba, “Adam: A method for stochastic optimization,” (2017), arXiv:1412.6980 [cs.LG].
- ⁵¹Initial parameters from ME+ICs.
- ⁵²Initial parameters from ME+ICs.
- ⁵³A. G. Baydin, B. A. Pearlmutter, A. A. Radul, and J. M. Siskind, “Automatic differentiation in machine learning: a survey,” *Journal of Machine Learning Research* **18**, 1–43 (2018).
- ⁵⁴Z. Yu, S. Ye, Y. Sun, H. Zhao, and X.-Q. Feng, “Deep learning method for predicting the mechanical properties of aluminum alloys with small data sets,” *Materials Today Communications* **28**, 102570 (2021).
- ⁵⁵F. Masi and I. Einav, “Neural integration for constitutive equations using small data,” *Computer Methods in Applied Mechanics and Engineering* **420**, 116698 (2024).
- ⁵⁶A. Vaswani, N. Shazeer, N. Parmar, J. Uszkoreit, L. Jones, A. N. Gomez, L. u. Kaiser, and I. Polosukhin, “Attention is all you need,” in *Advances in Neural Information Processing Systems*, Vol. 30, edited by I. Guyon, U. V. Luxburg, S. Bengio, H. Wallach, R. Fergus, S. Vishwanathan, and R. Garnett (Curran Associates, Inc., 2017).
- ⁵⁷Y. Yu, X. Si, C. Hu, and J. Zhang, “A Review of Recurrent Neural Networks: LSTM Cells and Network Architectures,” *Neural Computation* **31**, 1235–1270 (2019).
- ⁵⁸Z. Li, N. Kovachki, K. Azizzadenesheli, B. Liu, K. Bhattacharya, A. Stuart, and A. Anandkumar, “Fourier neural operator for parametric partial differential equations,” (2021).

Appendix A: Alternative loss for direct effect

An alternative loss function to enforce direct effect, inspired by the one used for healing, is also presented. It has not been implemented in the previous analyses, but

it is shown for completeness’ sake.

The magnitude of the jump in friction coefficient must be proportional to the logarithm of the ratio of final and initial velocities. Mathematically, we express that as

$$\begin{aligned} \mu(V_a) - \mu(V_b) &\propto \log\left(\frac{V_a}{V_b}\right) \\ \rightarrow \delta\mu_a - \delta\mu_b &\propto \log\left(\frac{V_a}{V_b}\right), \end{aligned} \quad (\text{A1})$$

where the sub-indices a and b refer to after and before the velocity jump. This is a physical constraint that does not have to be directly referred to the target values, but it is expressed as a condition that the predictions have to abide by. Thus, for all jumps during a virtual experiment, we should have

$$\left[\frac{\delta\mu_a - \delta\mu_b}{\log\left(\frac{V_a}{V_b}\right)} \right]_{J_1} = \dots = \left[\frac{\delta\mu_a - \delta\mu_b}{\log\left(\frac{V_a}{V_b}\right)} \right]_{J_{N_J}}, \quad (\text{A2})$$

where N_J refers to the total number of velocity jumps in any given velocity protocol, so J_1 means “first jump” and J_{N_J} “last jump”. Hence, the loss term that promotes the enforcement of the direct effect, expressed in this way, is:

$$\text{loss}_3 = \sum_{i=1}^{N_J-1} \left\{ \left[\frac{\delta\mu_a - \delta\mu_b}{\log\left(\frac{V_a}{V_b}\right)} \right]_{J_{i+1}} - \left[\frac{\delta\mu_a - \delta\mu_b}{\log\left(\frac{V_a}{V_b}\right)} \right]_{J_i} \right\}^2, \quad (\text{A3})$$

in other words, the magnitude of the friction coefficient change over any velocity jump must be the same across jumps.